First principle calculations of alkali hydride electronic structures

2007 J. Phys.: Condens. Matter 19 406211

(http://iopscience.iop.org/0953-8984/19/40/406211)

IOP PUBLISHING JOURNAL OF PHYSICS: CONDENSED MATTER

J. Phys.: Condens. Matter **19** (2007) 406211 (14pp) doi:10.1088/0953-8984/19/40/406211

First principle calculations of alkali hydride electronic structures

N Novaković[1], I Radisavljević[1], D Colognesi[2], S Ostojić[3] and N Ivanović[1]

[1] Institute for Nuclear Sciences 'VINČA', POB 522, 11001 Belgrade, Serbia
[2] Istituto dei Sistemi Complessi, Consiglio Nazionale delle Ricerche, Via Madonna del Piano 10, 50019 Sesto Fiorentino (FI), Italy
[3] Faculty of Technology and Metallurgy, Karnegijeva 4, 11120 Belgrade, Serbia

E-mail: nivanov@vin.bg.ac.yu

Received 29 March 2007, in final form 3 July 2007
Published 12 September 2007
Online at stacks.iop.org/JPhysCM/19/406211

Abstract

Electronic structure, volume optimization, bulk moduli, elastic constants, and frequencies of the transversal optical vibrations in LiH, NaH, KH, RbH, and CsH are calculated using the full potential augmented plane wave method, extended with local orbitals, and the full potential linearized augmented plane wave method. The obtained results show some common features in the electronic structure of these compounds, but also clear differences, which cannot be explained using simple empirical trends. The differences are particularly prominent in the electronic distributions and interactions in various crystallographic planes. In the light of these findings we have elaborated some selected experimental results and discussed several theoretical approaches frequently used for the description of various alkali hydride properties.

(Some figures in this article are in colour only in the electronic version)

1. Introduction

Alkali hydrides (AlkH for short) are materials of substantial practical [1] and theoretical [2–10] interest. The former arises from their recognized and potential applications in chemical and nuclear industries, and the latter from the fact that they are simple metal (M)–hydrogen (H) systems convenient for the investigations of fundamental interactions that are expected to be also important in new complex materials [11–13]. Although considerable experimental and theoretical work has been devoted to studying the AlkH, some of their essential features are not yet fully understood, for instance the details of valence and conduction bands and energy gap structures, the charge transfer and the charge distribution, the origin and the importance of various contributions to the bonding, and particularly the character and the importance of the H–H interaction. A full elaboration of these topics from the first principles is indispensable for our understanding of metal–H and H–H interactions in metallic systems in general. In addition,

numerous data about AlkH have been obtained and explained using various, and sometimes contradictory, concepts, so a coherent approach valid for all the properties along the AlkH series is still missing. Recent accurate experimental investigations, supported by appropriate calculations [14–16], have revealed apparent differences in the AlkH vibrational spectra, whose origin must be searched for in the details of the AlkH electronic structure. For these reasons we have performed detailed first principle calculations of the AlkH electronic structures using the full potential augmented plane waves extended with local orbitals (FP-APW + lo) and the full potential linearized augmented plane waves (FP-LAPW) methods, as implemented by the WIEN2k software package [17]. The obtained results are compared to some of the most frequently used theoretical concepts [5, 18–21], as well as to the existing experimental data.

2. Details of the calculations

All the calculations were spin unpolarized and performed using the FP-APW + lo/LAPW code based on the density functional theory (DFT). According to the method, the lattice space is divided into two regions: the atomic non-overlapping muffin-tin (MT) spheres and the interstitial space. Within the MT spheres the single-electronic states are defined by a standard APW+lo or LAPW basis set, with additional local orbitals defined as linear combinations of atomic-like radial functions and their first energy derivatives, which extend the variational flexibility of the calculations. In the interstitial space electronic states are described by plane waves. Core and valence states are separated by the MT criterion, which was adjusted so as to minimize the 'leakage' of the core state charge outside the MT spheres. Core states were treated fully relativistically, while valence states were treated within the scalar relativistic approximation. The effect of spin–orbital interactions was checked for RbH and CsH, and found to be irrelevant in the presented discussion. In an attempt to balance opposite requests concerning the H-ion muffin-tin sphere radii (R_{MT}), namely

(a) the small values of $R^{\mathrm{H}}_{\mathrm{MT}}$ (i.e. 0.4–0.6 Å) normally used in LAPW calculations of hydrogen-containing systems [22],
(b) the experimental observations of the considerably larger (around 1.3 Å) charge density distribution around H ions in AlkH [2, 7],
(c) the fact that the H charge density distribution remains almost constant (in range, but not in shape [5, 7]) in all the AlkH, and
(d) the practical recommendations on the MT sphere size for accurate WIEN2k calculations [23],

we have tried both $R^{\mathrm{H}}_{\mathrm{MT}} = 0.847$ and 0.953 Å for LiH and NaH, and 0.953 Å in all the other cases. The following figures have been employed for the R_{MT} values of various metal ions: $R^{\mathrm{Li}}_{\mathrm{MT}} = 0.847$ and 0.953 Å, $R^{\mathrm{Na}}_{\mathrm{MT}} = 1.058$ Å, $R^{\mathrm{K}}_{\mathrm{MT}} = 1.111$ Å, $R^{\mathrm{Rb}}_{\mathrm{MT}} = 1.164$ Å, and $R^{\mathrm{Cs}}_{\mathrm{MT}} = 1.164$ Å. The k-point sampling was done using the extended tetrahedron method [24] with 120 k-points in the irreducible wedge of the first Brillouin zone. The basis-set cut-off parameter $R_{\mathrm{MT}}K_{\mathrm{max}}$ (K_{max} being the maximal value of the plane wavevector in the interstitial region, and R_{MT} the radius of the smallest MT sphere in the system) was chosen to be seven in all cases. The magnitude of the largest vector in the charge density expansion, $G_{\mathrm{max}} = 14$, was enough for accurate calculations of all the AlkH. The influence of the exchange–correlation interaction was checked using different approximations, namely the generalized gradient approximation (GGA) [25] and the local density approximation (LDA) [26] in the case of KH. It was found that LDA calculations significantly underestimated the lattice constant of KH, so we have used the GGA approximation throughout the work. Another reason for choosing the GGA is that more LDA than GGA results on these systems already exist (see table 1 and corresponding

Table 1. Selected calculated and experimental properties of alkali hydrides. a is the lattice constant, B is the bulk modulus, γ is the Grüneisen parameter, C_{ij} are the elastic constants, $C' = (C_{11} - C_{12})/2$, and ω_{TO} is the transversal optical frequency at the gamma point.

	a (Å)	B (GPa)	$\partial B/\partial p$	γ	C' (GPa)	C_{11} (GPa)	C_{12} (GPa)	C_{44} (GPa)	C_{12}/C_{44}	ω_{TO} (10^{14} s^{-1})
LiH	4.009	33.9	1.97	0.82	36.9	84.8	11.1	48.0	0.23	1.156
	4.075 [7][a]	35.7[b]			30.0 [6]	74.1 [6][a]	14.2 [6][a]	48.1 [6][a]	0.30 [6]	0.855 [6]
	4.069 [27][a]	32.3 [30][b]		1.2 [30][a]	26.2 [30]	67.2 [30][a]	14.8 [30][a]	46.1 [30][a]	0.32 [30]	
	4.084 [28][a]	40.5 [31][b]			27.3 [31]	76.9 [31]	22.3 [31]	51.7 [31]	0.43 [31]	
		34.1 [8]								1.84 [8]
		33.6 [10]								0.766 [35]
		32.2 [28][a]	3.53 [28][a]							0.115 [4][a]
		40.5 [43][b]			45.3 [43]	100.9 [43]	10.3 [43]	51.4 [43]	0.20 [43]	
NaH	4.842	24.08	8.26	3.96	22.3	52.5	8.0	20.7	0.39	0.959
	4.880 [27][a]	22.8[b]								0.870 [4]
		30.8 [6][b]			12.4 [6]	47.3 [6]	2.5 [6]	22.5 [6]	1 [6]	0.799 [6]
		19.7 [8]								0.852 [8]
		27.4 [31][b]			12.3 [31]	43.8 [31]	19.2 [31]	26.1 [31]	0.74 [31]	0.275 [35]
		29.6 [43][b]			20.5 [43]	56.9 [43]	15.9 [43]	24.7 [43]	0.64 [43]	
		14.3 [32][a]	7.7 [32][a]							
		23.5 [33]	3.16 [33]							
		19.4 [34][a]	4.4 [34][a]							
KH	5.705	14.3	3.1	1.38	6.8	23.0	9.4	10.3	0.9	0.790
		13.9[b]								0.755 [4]
	5.471[c]	17.54 [c,b]	4.16[c]	1.91[c]	16.9[c]	38.5[c]	4.7[c]			0.387 [35]
		16.0[b]								
	5.700 [27][a]	16.3 [31][b]			12.4 [31]	32.8 [31]	8.04 [31]	12.9 [31]	0.62 [31]	
		17.3 [43][b]			16.6 [43]	39.4 [43]	6.3 [43]	10.4 [43]	0.6 [43]	
		15.6 [32][a]	4.0 [32][a]							
RbH	6.075	11.84	2.16	0.92	3.45	16.5	9.6	6.9	1.39	0.754
	6.037 [27][a]	10.1[b]								0.654 [4]
		14.1 [31][b]			10.6 [31]	28.2 [31]	7.11 [31]	12.5 [31]	0.57 [31]	0.307 [35]
		14.7 [43][b]			15.3 [43]	35.1 [43]	4.5 [43]	7.6 [43]	0.6 [43]	
		10.0 [32][a]	3.9 [32][a]							
CsH	6.409	10.13	2.96	1.32	4.60	16.4	7.2	6.7	1.08	0.726
	6.376 [27][a]	9.2[b]								0.275 [35]
		8.8 [31][b]			8.6 [31]	20.3 [31]	3.1 [31]	9.1 [31]	0.34 [31]	
		7.6 [32][a]	4.0 [32][a]							
	6.388 [29][a]	11.9 [43][b]			16.1 [43]	33.4 [43]	1.2 [43]	4.7 [43]	0.26 [43]	
		8.0 [29][a]	4.0 [29][a]							

[a] Experimental estimates.
[b] Values are calculated from $B = (C_{11} + 2C_{12})/3$.
[c] LDA results.

references therein). The charge difference of $10^{-5}e$ in two consecutive iterations was found to be a more reliable convergence criterion than the default one concerning the energy difference of 10^{-4} Ryd. Energy versus volume optimization was performed for all the systems under investigation. The elastic constants C_{11}, C_{12} and C_{44} were also calculated from first principles. For RbH and CsH the FP-LAPW basis set was used to obtain accurate results for all of the three different lattice distortions. During these calculations in RbH, the low-lying 3d states

Table 2. Some characteristic energies in AlkH: E_{SM} and E_{SH} are the atomic s levels of metal (M) and hydrogen (H) [19], $\alpha e^2/d$ is the enhancement of the Madelung energy due to the M-to-H charge transfer, $\Delta E = U(H) - \alpha e^2/d$ is the effective energy change due to the M-to-H charge transfer, with $U(H) = 12.851$ eV; E_g, E_{coh}, E_{vb}, and ΔH_f are the energy gap, the cohesive energy, the valence band width, and the enthalpy of formation, respectively.

	$E_{SM}-E_{SH}$ (eV)	$\alpha e^2/d$ (eV)	$E_{SM}-E_{SH}-\Delta E$ (eV)	E_{coh} (eV)	E_g (eV)	E_{vb} (eV)	ΔH_f (kJ mol^{-1})
LiH	8.26	12.58	7.99	5.04	3.03	5.40	−92.1
				9.38 [2][a]	4.92 [10]	5.21 [10]	−87 [40]
				8.13 [5]	6.61 [20]		−90.5 [40][a]
					9.15 [21]	13 [21]	
					3.31 [23]		
					4.99 [36, 37][a]		
					4.4 [38][a]	6.0 [38][a]	
					9.2 [39][a]	6 [39][a]	
NaH	8.64	10.42	6.21	6.83	3.77	3.55	−59.0
				8.22 [2][a]	1.52 [20]		−43 [40]
				7.56 [5]	3.46 [35]		−56.3 [40][a]
KH (LDA)	9.59	8.82	5.56	5.07	3.44	1.84	−70.4
				7.22 [2][a]	(3.04)	(2.27)	−41 [40]
				6.28 [5]	3.203 [35]		−57.7 [40][a]
RbH	9.85	8.29	5.29	4.21	2.92	1.81	−49.9
				6.97 [2][a]	2.96 [35]		
CsH	10.23	7.90	5.28	4.04	2.34	1.67	−45.5
				6.67 [2][a]	2.80 [33]		

[a] Experimental estimates.

were excluded from the valence panel. The frequency of the transversal optical vibrations ω_{TO} at the gamma point was derived using the forces obtained from H-atom displacements from their equilibrium lattice positions along the appropriate direction (i.e. M–H–M).

3. Results

The volume optimization curves were used to calculate the lattice constants a, the bulk moduli B, their derivatives $\partial B/\partial p$, and the Grüneisen parameters γ of all the AlkH structures. Grüneisen parameters were evaluated according to the formula [19]

$$\gamma = \frac{1}{2}\left(\frac{\partial B}{\partial p} - \frac{1}{3}\right).$$

Calculated elastic constants were used to derive the tetragonal shear constant $C = (C_{11} - C_{12})/2$ and the Cauchy ratio C_{12}/C_{44}. All these quantities, together with a short overview of the corresponding experimental and calculated values, are reported in table 1. In table 2, some characteristic energies of AlkH are presented. The enthalpy of formation was calculated as

$$\Delta H_f = \tfrac{1}{2}(2E_{MH} - 2E_M - E_{H_2}).$$

E_{MH} is the AlkH ground state energy, E_M is the ground state energy of the metal and E_{H_2} is that of the hydrogen molecule. Cohesive energy was calculated according to the formula

$$E_{coh} = (E_M^a + E_H^a) - E_{MH}.$$

E_M^a and E_H^a are the energies of an isolated metal and hydrogen atom, respectively.

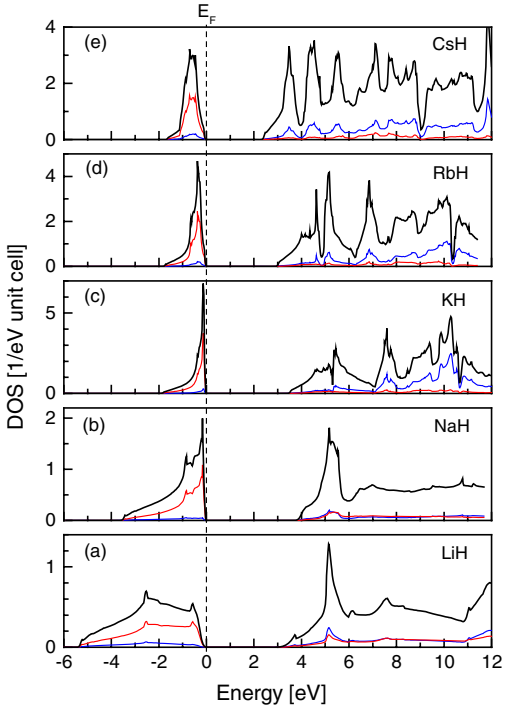

Figure 1. Calculated total DOS for LiH (a), NaH (b), KH (c), RbH (d), and CsH (e) (solid line). The dotted (red) line is the H contribution; the dashed (blue) line is the M contribution. The Fermi level is set to zero energy and marked by the vertical dashed line.

The total and atomic site-decomposed electron densities of states (DOSs) of the investigated AlkH are presented in figure 1. In figure 2 one can see the s-projected, and in figure 3 the p-projected DOS in the H (solid/red line) and M (dotted/blue line) positions, for all the AlkH. The main contributions to the valence band (see figures 2 and 3) are provided in order of relevance by H s, M p, and M s states. The structure of the first peak in the conduction band (see figure 1) is similar for LiH and NaH, but different for KH, and further. In the first three AlkH compounds it mainly consists of M p, H p, and M s states, with an additional and large d contribution in RbH and CsH.

The charge distribution in the ⟨100⟩ plane, containing M^+ and H^- ions, is reported in figure 4(a). In this plane one can detect charge concentrations along the M–H bonds in all the AlkH. In the LiH case the voids (i.e. charge depletion regions) are narrow between H ions and broad between Li ions. By increasing the M-ion atomic number the M–H bonding becomes weaker, and these voids change their shape. They are almost symmetric in NaH and KH, and they turn asymmetric again in RbH and CsH, but in a different way: narrow between M ions and broad between H ions. This peculiar behaviour reflects the ionic distances and character of the bonding interactions in the lattice of the various AlkH. More details of the charge distribution in the ⟨100⟩ plane can be seen in figure 4(b), in which the difference between the sum of the atomic charges, and the charge obtained from the presented FP-APW + lo calculations, is given. This difference is usually considered [33] as a good indication of the charge directly involved in the bonding. Several intriguing features are present in this figure. Due to the rise of the close-shell repulsion the M^+–H^- distance increases faster, while the M^+–M^+ distance increases more slowly, than the M^+ ion size. This approaching of the M^+-ion outer shells is

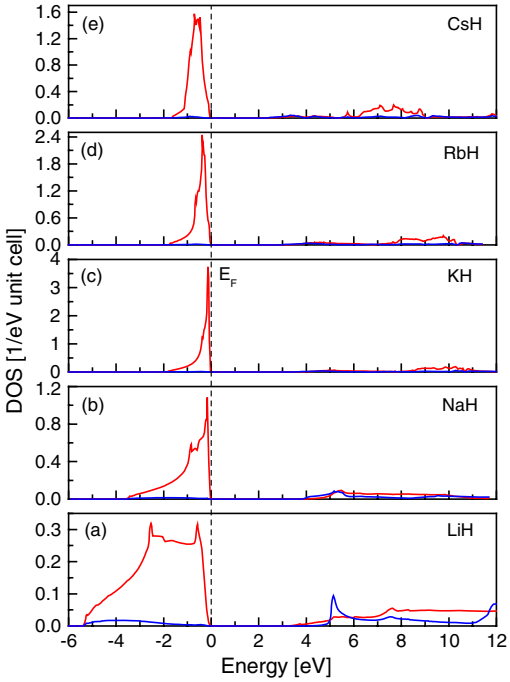

Figure 2. Calculated s-DOS on H (solid/red line) and M (dotted/blue line) atoms, for LiH (a), NaH (b), KH (c), RbH (d), and CsH (e). The Fermi level is set to zero energy and marked by the vertical dashed line.

accompanied by an increase of the excess charge between M^+ and H^- ions in the ⟨100⟩ plane, which at first glance seems to contradict the results presented in figure 4(a) and all the other results of this investigation concerning the M^+–H^- bonding in AlkH.

In figure 5(a) the charge distribution in the ⟨111⟩ plane, containing only M^+ ions, is presented. One can see that, as in the ⟨100⟩ plane (figure 4(a)), the M–H bonds in the ⟨111⟩ plane also become gradually weaker as the M atomic number increases. In LiH a clear sign of the H–H bonding is evident in the charge distribution of this plane: bonds are obviously using some of the Li charge. In NaH, the voids in the charge distribution between the H ions that exist in the ⟨100⟩ plane (see figure 4(a)) spread in the ⟨111⟩ plane too, and suppress the H–H bonding. In KH and beyond, the increase of the M^+ size reduces the M^+–M^+ distance, and, as can be seen in figure 4(b), compresses and localizes the charge distribution toward the ⟨100⟩ plane, depleting the M^+–M^+ inter-atomic region in the ⟨111⟩ plane in a characteristic way. In CsH, both Cs^+ and H^- on one side, and Cs^+ and Cs^+ on the other, are almost in direct contact, providing a charge distribution unique in the AlkH sequence and totally different from the LiH case. More details about charge distribution in the ⟨111⟩ plane can be seen in figure 5(b), where the difference between the sum of the atomic charges, and the charge obtained from the FP-APW + lo calculations, is presented. One can see that in LiH and NaH a substantial excess charge in this plane is located over the H atoms. In KH and RbH this plane is almost completely depleted of the excess charge and, in addition, in CsH the Cs atoms are in immediate contact with each other.

The charge distribution in the ⟨222⟩ plane (containing H ions only) is plotted in figure 6(a), together with the difference between the sum of the atomic charges, and the charge obtained

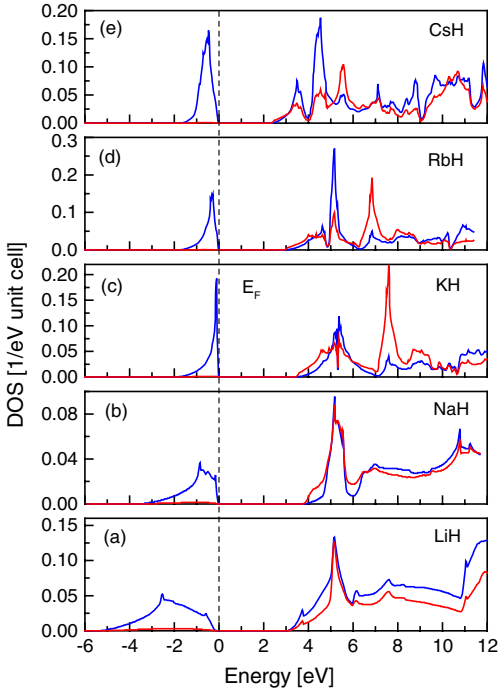

Figure 3. Calculated p-DOS on H (solid/red line) and M (dotted/blue line) atoms for LiH (a), NaH (b), KH (c), RbH (d), and CsH (e). The Fermi level is set to zero energy and marked by the vertical dashed line.

from the FP-APW + lo calculations (figure 6(b)). In figure 6(a) the M–H bonds dominate again, and a tendency for H to use some of the metal charge is visible as well. The general features of the charge distribution in this plane are very similar for LiH and NaH, and in an essentially different way for RbH and CsH, with KH being once more a crossover case. The voids between the H^- ions become gradually larger as the M^+ size increases. These features are expressed in figure 6(b) too. One can see a weak but real charge concentration between the H^- ions in LiH, which vanishes in NaH. In KH these voids between H^- ions persist, but the charge in this plane accumulates above the metal (K^+) ions. In RbH and CsH, the atomic charges of M^+ and H^- ions are in direct contact, not only in the ⟨100⟩ nearest neighbour plane (figures 4(a) and (b)), but also in the ⟨222⟩ plane (figure 6(b)).

In figure 7 the three-dimensional charge distributions of LiH and NaH are presented. The situation, already observed in previous figures, is here even more transparent: the voids in the distribution between H ions in LiH are the explicit confirmation of the existence of the H–H bonding in this system. This feature is absent from all the other AlkH, although differences among them are visible through the relative sizes of M^+ and H^- ions, the extension of the charge distribution around them and dimensions of the voids between M^+–M^+ and M^+–H^- ions, which are related to the charge involved in the bonding.

To clarify the influence of the charge distribution peculiarities on the properties of AlkH in more detail, in figure 8 we present the charge distributions along the relevant crystallographic directions. Clearly, the lattice constant does not follow monotonically the increase of the M^+-ion atomic number, at least to the first neighbour interaction, in full agreement with the situation presented in figures 4–7.

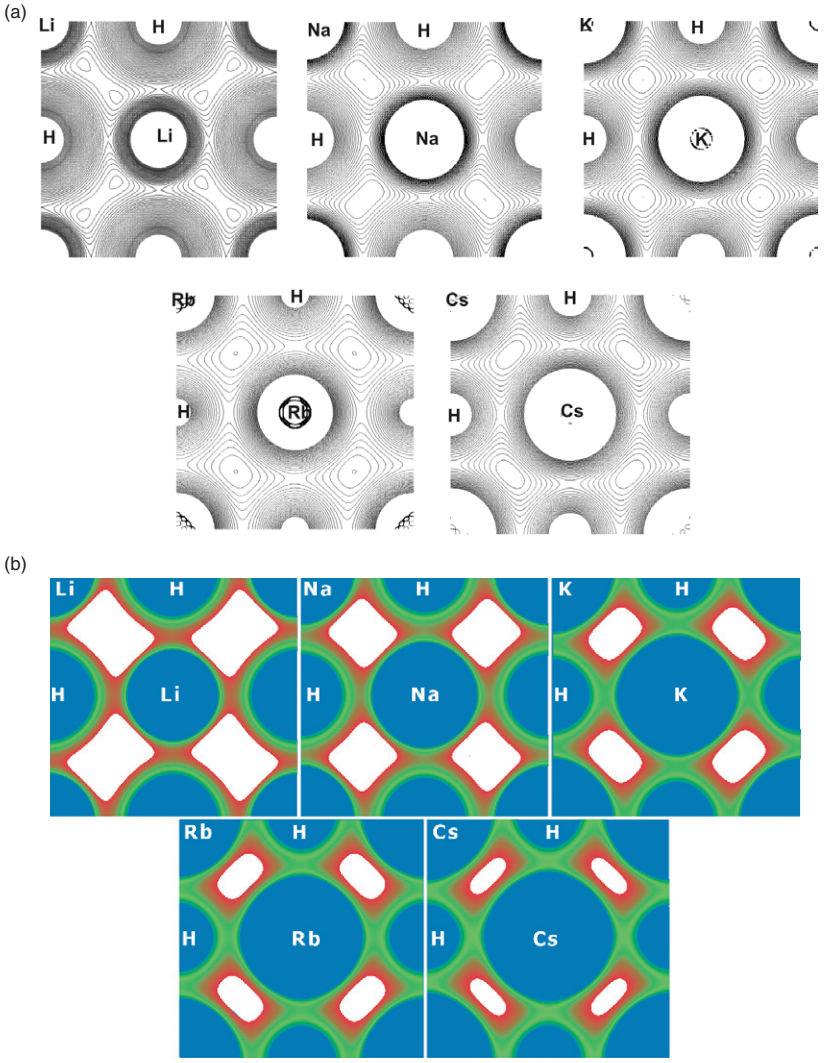

Figure 4. (a) Calculated charge distribution in the ⟨100⟩ plane for LiH (a), NaH (b), KH (c), RbH (d), and CsH (e). (b) Differences between the sum of the atomic charges and the calculated crystal charge in the ⟨100⟩ plane of LiH (a), NaH (b), KH (c), RbH (d), and CsH (e). Only the regions with a negative charge difference (accumulation) are coloured. White corresponds to a positive charge difference (depletion). The increase of the excess charge is presented by changing the colour from red to blue (shading from black (maximal depletion) to white (zero depletion) in the printed version).

4. Discussion

According to our calculations, and similarly to [35], E_g reaches its maximum value in the AlkH series for NaH, in evident contradiction with the low value found in [20]. The comparison between calculated and experimental E_g data (see table 2) shows that the former are obviously underestimated, as is usual in DFT calculations [41]. But the existing experimental [36–39] and theoretical [8, 9, 20, 21, 35] estimates are also largely uncertain and fluctuating, so that a final conclusion about E_g requires an additional careful analysis. However, the inaccuracy in the

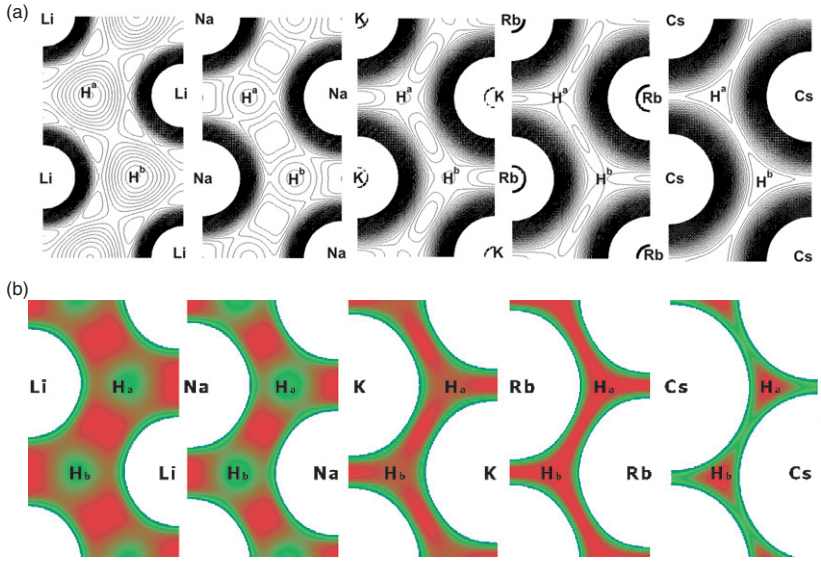

Figure 5. (a) Calculated charge distribution in the ⟨111⟩ plane for LiH (a), NaH (b), KH (c), RbH (d), and CsH (e). H^a hydrogens are above, while H^b hydrogens are below the ⟨111⟩ plane. (b) Differences between the sum of the atomic charges and the calculated crystal charge in the ⟨111⟩ plane of LiH (a), NaH (b), KH (c), RbH (d), and CsH (e). Only the regions with a positive charge difference are coloured. White corresponds to a negative charge difference (accumulation). The increase of the excess charge is presented by changing the colour from red (maximal depletion) to blue (zero depletion) (shading from black (maximal depletion) to white (zero depletion) in the printed version).

DFT evaluation of E_g in ionic and covalent systems is usually a consequence of a rigid shift of the conduction band [41], which is comparable for similar systems, so the obtained trend should be much more reliable than the absolute values of E_g. The principal difference between E_g and E_{coh} in ionic systems derives from the Coulomb gap broadening, which does not affect E_{coh}. The different trends of E_{coh} and E_g along the AlkH series (see [2, 5] data in table 2) imply the existence of a significant amount of non-ionic contribution to the bonding in the light AlkH, probably the non-vanishing covalent M–H contribution, and at least in LiH an evident H–H resonant bonding (see figures 5 and 7). Our E_{coh} and E_g results (table 2) follow a similar trend, indicating that the aforementioned effects have been taken into account by the *ab initio* self-consistent GGA calculations, which provides additional confidence to the obtained E_g trend. The calculated valence bandwidth E_{vb} is close to the results obtained experimentally [38, 39]. It is largest for LiH (but narrower and more peaked near the Fermi energy E_F than the LDA results of [9]) and decreases along the series, steeply from LiH to KH, and then in a smoother way. These trends are related to the charge distribution features presented in figures 4–7.

The significant M-p contribution to the valence band found by the present calculations corrects the frequently used picture [5, 9, 36, 38] of an AlkH valence band mainly composed of the (hybridized) H-s and M-s states. The relative contribution of the M states to the valence band, and consequently to bonding, is considerable larger in LiH than in the other AlkH, being minimal for KH and NaH, owing to their large E_g values. The number of valence-band H-s states is the lowest in the series for NaH, and maximal for KH. Due to the significant involvement of d states, the M-state contribution to the valence band in RbH and CsH increases again. This complex behaviour is related to the degree and the details of the H–M hybridization, which appears to be quite different among the AlkH, especially in some crystallographic planes.

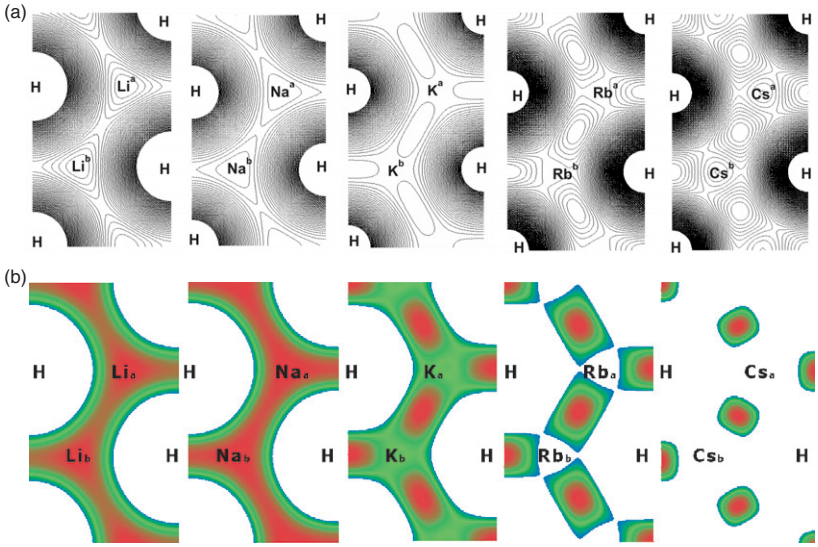

Figure 6. (a) Calculated charge distribution in the ⟨222⟩ plane for LiH (a), NaH (b), KH (c), RbH (d), and CsH (e). M^a metal ions are above, while M^b metal ions are below the ⟨222⟩ plane. (b) Differences between the sum of atomic and calculated crystal charge in the ⟨222⟩ plane of LiH (a), NaH (b), KH (c), RbH (d), and CsH (e). Only the regions with a positive charge difference are coloured. White corresponds to a negative charge difference (accumulation). The increase of the excess charge is presented by changing the colour from red (maximal depletion) to blue (zero depletion) (shading from black (maximal depletion) to white (zero depletion) in the printed version).

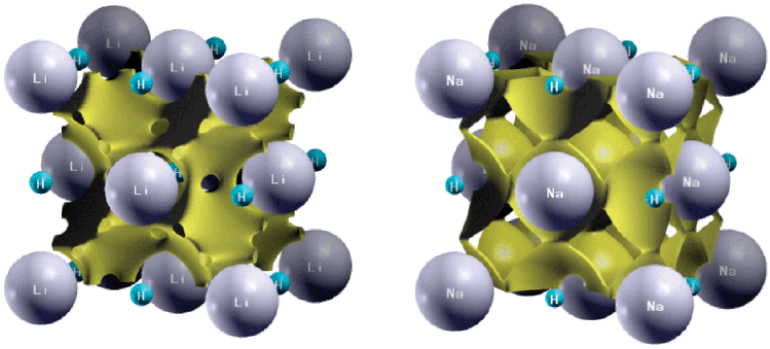

Figure 7. Calculated three-dimensional charge distribution in LiH (a) and NaH (b) [42].

The H states in LiH are considerably more coupled to the metal ones than in the other AlkH. This fact enables the charge delocalization and makes the resonant H–H interaction in LiH possible, a unique feature in the series. These collective bonding effects involve in LiH more atoms than in the other AlkH, making the LiH valence band much broader, and significantly enhancing the LiH stability.

Our results confirm previous findings [20, 21, 36, 38, 39] about the p character of the AlkH conduction band minimum. However, there are some differences in the structure of the various conduction band peaks along the AlkH series. In LiH and NaH the H-s contribution to the conduction band minimum is not negligible. In KH, RbH, and CsH, the main H-p contribution

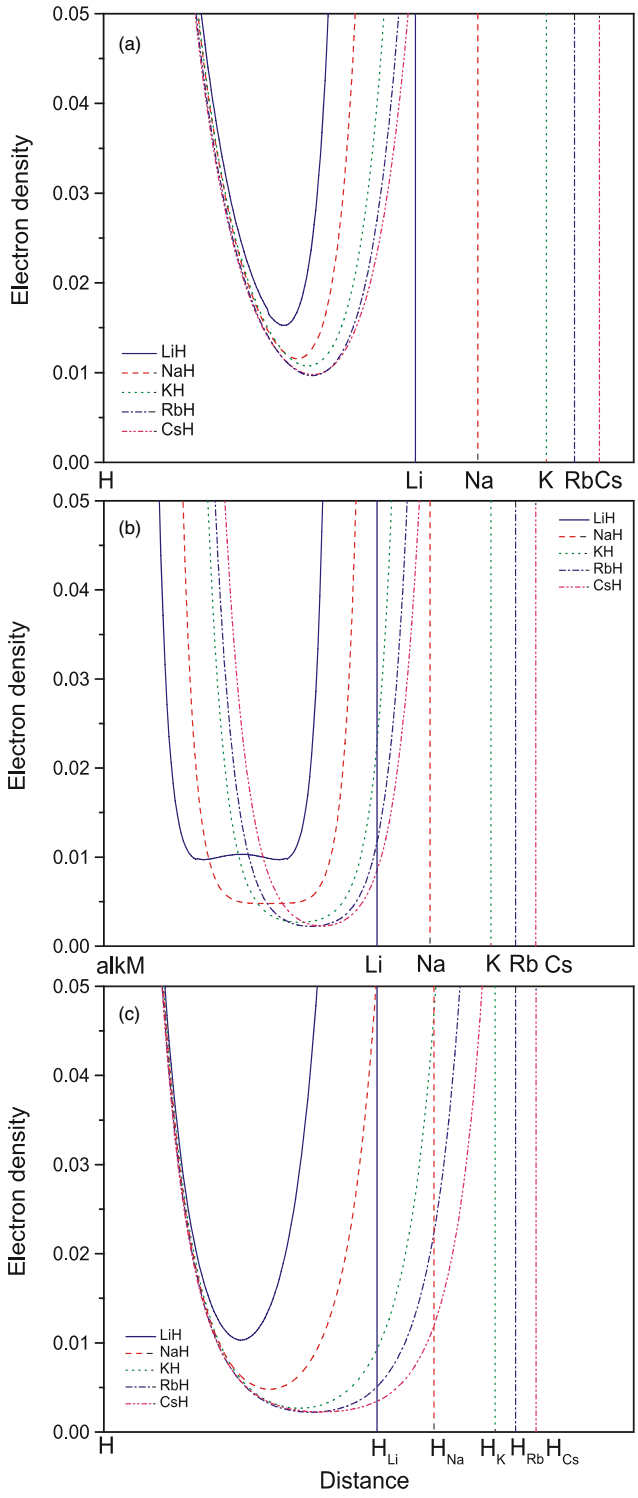

Figure 8. Electron density plots between (a) H^- and M^+ ions in the ⟨100⟩ plane, (b) M^+ and M^+ ions in the ⟨111⟩ plane, and (c) H^- and H^- ions in the ⟨222⟩ plane.

is shifted away from the conduction band minimum, toward higher energies, and in RbH and CsH the d contribution to the conduction band is larger than the s and p ones. The hybridization generally weakens from KH to CsH and the distinct contributions from the atomic states are better resolved in separate peaks, supporting the picture of more compact and better resolved ions in the heavier AlkH, despite their proximity in the lattices of RbH and CsH.

The LDA approximation for the exchange–correlation effects was tested for KH only. It significantly underestimates the KH lattice constant (see table 1) and makes the already small E_g value even smaller. It provides a reasonable estimate of the bulk modulus, but gives a too high C_{11}, and a too low C_{12} elastic constant. LDA broadens the valence band and enhances the first peak in the conduction band transferring to it some of the valence-band K-p and H-p states, promoting in this way the non-directional s–s contribution to the lattice cohesion. These results point out the importance of a proper choice of the form of the exchange–correlation interaction for the correct description of these compounds, a fact already noticed in [10, 21, 43].

Figures 4–6 clearly show that the features of the M–H hybridization are essential for both the strength of the M–H bonding and the details of the second neighbour interaction, the latter being particularly prominent between H ions in LiH. However, our results suggest that the principal variations in AlkH bonding do not originate from the existing excess charge accumulation in the M–H ⟨100⟩ crystallographic plane (figure 8). According to figures 4(a) and (b) this excess charge originates mainly from the non-bonding atomic charge superposition. The total inter-ionic charge in this, but also in the other two investigated planes, is the largest in LiH (figure 8). It is appreciably less intense in NaH, and additionally slightly lower in KH, RbH, and CsH than in NaH, being almost identical in the last three compounds. However, the excess charge between M^+ and H^- ions follows an exactly opposite trend, increasing from LiH to NaH, and further for KH, RbH, and CsH, being again almost identical in the last three compounds. Obviously, the increase of the M^+ ion radius leads to the compression of the excess charge in the ⟨100⟩ plane. The saturation of this effect going from KH to CsH is probably a consequence of the low level of their initial inter-ion charge, e.g. their more pronounced ionic character. Most of the bonding charge in the M–M ⟨111⟩ plane in LiH and NaH is accumulated above (and under) the H ions, a feature completely absent from the heavier AlkH (see figures 5(a) and (b)). Apparently, the H–H second neighbour interaction in LiH is established over the M–M ⟨111⟩ plane, and is more metallic (delocalized) than covalent (directional) in nature, the 'metallic' character of the bonding charge being strictly confined to the ⟨111⟩ crystallographic plane. The charge distribution in ⟨111⟩ is complemented by the charge distribution in the H–H ⟨222⟩ plane, in a way that equalizes both the inter-atomic distances (a necessary condition for the lattice periodicity) and the charge distribution levels between essentially different ions: M^+–M^+ in the ⟨111⟩ and H^-–H^- in the ⟨222⟩ plane. In the ⟨222⟩ plane of LiH a weak charge accumulation between H ions exists, while the space over the Li^+ ions is depleted. The plane is completely depleted of the excess charge in NaH, and for KH and further the charge accumulates over M^+ ions, establishing an immediate contact between M^+ and H^- ions in RbH and CsH, not only in ⟨100⟩, but also in this plane.

The M–H bond-weakening trend going from LiH to CsH can be derived explicitly from the values of the Γ-point phonon frequency of the optic transverse branch, ω_{TO}, since in AlkH it is essentially related to the M and H anti-phase motion in the lattice unit cell. Despite the large scattering of the various ω_{TO} estimates reported in table 1, one can clearly infer a frequency softening as the metal atomic number grows. This trend has also been recently confirmed by incoherent inelastic neutron scattering measurements on the complete AlkH series [16], where not only is the Γ-point explored, but all the ω_{TO} values in the first Brillouin zone. The various importance of the further neighbours interaction in AlkH can be also judged from the values of the Cauchy ratio (table 1) and from the difference between the longitudinal ω_{LO} and transversal

ω_{TO} optical phonon frequencies, which decreases in AlkH with the M-ion size [14, 16, 43]. It is important to stress again that both shear moduli in LiH are large, and the main reason for a low Cauchy ratio is the significant H–H second neighbour interaction. Unlike in [31, 43], our Cauchy ratio value for NaH is also quite low, but, as one could expect, it moves toward the ideal value of unity for the heavier and more ionic KH, RbH, and CsH. These results are sensible and in agreement with the trends observed in the charge distributions and in the optical vibrational modes. The low Cauchy ratio values observed for RbH and CsH in [31, 43] are probably calculation flaws. Our calculations show that the FP-APW + lo method does not provide accurate values of elastic constants for RbH and CsH, and that quite large FP-LAPW basis sets and a careful consideration of the Rb and Cs d states are necessary for reliable results. In addition, in RbH and CsH the close proximity of M^+ ions in the $\langle 111 \rangle$ crystallographic plane enables a significant repulsive interaction, which causes both shear moduli to be low in these compounds.

5. Conclusions

We have presented detailed FP-APW + lo and FP-LAPW calculations of the LiH, NaH, KH, RbH and CsH (AlkH in short) electronic structures. These calculations clearly reveal that the experimentally observed discrepancies in the behaviour of these compounds have their origin in the peculiarities of their electronic structure. Although the AlkH are often considered as simple ionic compounds of similar characteristics, the presented calculations show that for each of them there is at least one electronic feature which is unique in the particular compound and differs from the general trend. This is true especially for the charge distributions in distinct crystallographic planes of various AlkH. The improved stability of LiH is a collective band effect. It is a consequence of the enhanced bonding between Li and H, and of a resonant bonding among the H ions, which is enabled by the peculiar charge distribution in the LiH $\langle 111 \rangle$ plane. In addition, the almost complete compensation of the two electrostatic contributions to the lattice energy, the electrostatic repulsion of the excess electron in the H-ion position and the gain in the Madelung energy obtained from this electron transfer (table 2), minimizes the competition between the lattice constant and the ion size in LiH. Due to the actual ion size, which influences both the lattice constant and the Madelung interaction, and the specific distribution of the M atomic levels included in the compound formation, this effect is suppressed in the other AlkH. The H–H bonding is absent already from NaH, and the resonant M–H bonding becomes weaker moving towards the AlkH including heavier metallic ions. However, the electrostatic interplay between the ion size and the lattice persists, expressed by the fact that the lattice expansion does not regularly follow the increase of the M-ion radius, which leads to the enhanced charge compression around the ions in KH, RbH, and CsH, and a more pronounced ionic character of these compounds. This behaviour is also exposed in the values and relations between some macroscopic parameters like the elastic constants and the optical vibrational frequencies. The consequences of the resonant H–H bonding in LiH should reveal itself in various interesting phenomena. For instance, due to the prominent H–H interaction, the 'effective charges' localized on Li and H ions should be different, a possibility that is accounted for by none of the existing models. Moreover, the H–H bonding must be considered as an additional collective interaction existing in LiH, leading to a collective response of the H-ion sub-lattice. Some of these specific features of the LiH charge distribution are experimentally observed, and they seems to break the validity of the Born–Oppenheimer approximation, making the LiH vibrational spectrum peculiar if compared to the NaH, and especially to the KH, RbH, and CsH ones. Further investigations of these intriguing aspects of the AlkH physical properties are in progress.

Acknowledgments

The financial support of this work by the Serbian Ministry of Science under grant 141009B is gratefully acknowledged.

References

[1] Islam A K M A 1993 *Phys. Status Solidi* b **180** 9 and references therein
[2] Bowman R C 1971 *J. Phys. Chem.* **75** 1251
[3] Ruffa A R 1983 *Phys. Rev.* B **27** 1321
[4] Hussain A R Q and Sangster M J L 1986 *J. Phys. C: Solid State Phys.* **19** 3535
[5] Luaña V and Pueyo L 1990 *Phys. Rev.* B **41** 3800
[6] Haque E and Islam A K M A 1990 *Phys. Status Solidi* b **158** 457
[7] Vidal-Valat G, Vidal J-P, Kurki-Suonio K and Kurki-Suonio R 1992 *Acta Crystallogr.* A **48** 46
[8] Blat D Kh, Zein N E and Zinenko V I 1991 *J. Phys.: Condens. Matter* **3** 5515
[9] Smithson H, Marianetti C A, Morgan D, Van der Ven A, Predith A and Ceder G 2002 *Phys. Rev.* B **66** 144107
[10] Lebegue S, Alouani M, Arnuad B and Pickett W E 2003 *Europhys. Lett.* **63** 562
[11] Bogdanović B and Schwickardi M 1997 *J. Alloys Compounds* **253/254** 1
[12] Bogdanović B, Brand R A, Marjanović A, Schwickardi M and Tölle J 2000 *J. Alloys Compounds* **302** 36
[13] Vajeeston P, Ravindran P, Vidya R, Fjellvåg H and Kjekshus A 2003 *Appl. Phys. Lett.* **82** 2257
[14] Boronat J, Cazorla C, Colognesi D and Zoppi M 2004 *Phys. Rev.* B **69** 174302
[15] Colognesi D, Ramirez-Cuesta A J, Zoppi M, Senesi R and Abdul-Redah T 2004 *Physica* B **350** e983
[16] Auffermann G, Barrera G D, Colognesi D, Corradi G, Ramirez-Cuesta A J and Zoppi M 2004 *J. Phys.: Condens. Matter* **16** 5731
[17] Blaha P, Schwarz K, Madsen G K H, Kvasnicka D and Luitz J 2001 *WIEN2k An Augmented Plane Wave + Local Orbitals Program for Calculating Crystal Properties* (K Schwarz, Techn. Universtät, Wien, Austria) ISBN 3-9501031-1-2
[18] Pettifor D G 1995 *Bonding and Structure of Molecules and Solids* (Oxford: Clarendon)
[19] Harrison W A 2004 *Elementary Electronic Structure* (Singapore: World Scientific)
[20] Kunz A B and Mickish D J 1975 *Phys. Rev.* B **11** 1700
[21] Grosso G and Parravicini G P 1979 *Phys. Rev.* B **20** 2366
[22] Ambrosch-Draxl C, Majewski J A, Vogl P and Leising G 1995 *Phys. Rev.* B **51** 9668
[23] Blaha P, Schwarz K, Madsen G K H, Kvasnicka D and Luitz J 2001 *WIEN2k User's Guide* http://www.WIEN2k.com
[24] Blöchl P E, Jepsen O and Andersen K O 1994 *Phys. Rev.* B **49** 16223
[25] Perdew J P, Burke S and Ernzerhof M 1996 *Phys. Rev. Lett.* **77** 3865
[26] Perdew J P and Wang Y 1992 *Phys. Rev.* B **45** 13244
[27] Wyckoff R W G 1963 *Crystal Structures* vol I (New York: Interscience)
[28] Loubeyre P, LeToullec R, Hanfland M, Ulivi L, Datchi F and Hausermann D 1998 *Phys. Rev.* B **45** 2613
[29] Ghandehari K, Luo H and Ruoff A L 1995 *Phys. Rev. Lett.* **74** 2264
[30] James B W and Kheyrandish J 1982 *J. Phys. C: Solid State Phys.* **15** 6321
[31] Engebretsen L 1995 Electronic structure calculations of the elastic properties of alkali hydrides *Graduation Thesis* Royal institute of technology KTH, Stockholm
[32] Hochheimer H D, Strössner K and Hönle W 1985 *J. Less-Common Met.* **107** L13
[33] Vajeeston P 2004 Theoretical modeling of hydrides *PhD Thesis* University of Oslo
[34] Duclos J, Vohra Y K, Ruoff A L, Filipek S and Baranowski B 1987 *Phys. Rev.* B **36** 7664
[35] Zinenko V I and Fedorov A S 1994 *Sov. Phys.—Solid State* **36** 742
[36] Zavt G S, Kalder K A, Kuusmann I L, Lushchik Ch B, Plekhanov V G, Cholakh S O and Evarestov P A 1976 *Sov. Phys.—Solid State* **18** 1588
[37] Plekhanov V G, Pustovarov V A, O'Connel-Bronin A A, Betenekova T A and Cholakh S O 1976 *Sov. Phys.—Solid State* **18** 1422
[38] Betenekova T A, Cholakh S O, Shabanova I M, Trapeznikov V A, Gavrilov F F and Shulgin B V 1978 *Sov. Phys.—Solid State* **20** 1426
[39] Ichikawa K, Suzuki N and Tsutsumi K 1981 *J. Phys. Soc. Japan* **50** 3650
[40] Wolverton C, Ozoliņš V and Asta M 2004 *Phys. Rev.* B **69** 144109
[41] Zhu X and Louie S G 1991 *Phys. Rev.* B **43** 14142
[42] XCRYSDEN program, see Kokalj A 1999 *J. Mol. Graph. Modelling* **17** 176
[43] Barrera G D, Colognesi D, Mitchell P C H and Ramirez-Cuesta A J 2005 *Chem. Phys.* **317** 119